

RESEARCH ARTICLE

In Vitro and *In Vivo* Evaluation of the Caspase-3 Substrate-Based Radiotracer [^{18}F]-CP18 for PET Imaging of Apoptosis in Tumors

Chun-Fang Xia, Gang Chen, Umesh Gangadharmath, Luis F. Gomez, Qianwa Liang, Fanrong Mu, Vani P. Mocharla, Helen Su, A. Katrin Szardenings, Joseph C. Walsh, Tieming Zhao, Hartmuth C. Kolb

Molecular Imaging Biomarker Research, Siemens Medical Solutions USA, Inc., 6100 Bristol Parkway, Culver City, CA, 90230, USA

Abstract

Purpose: A novel caspase-3 substrate-based probe [^{18}F]-CP18 was evaluated as an *in vivo* positron emission tomography (PET) imaging agent for monitoring apoptosis in tumors.

Methods: Uptake of [^{18}F]-CP18 in cell assays and tumors was measured. Caspase-3/7 activities in cell lysates and tumor homogenates were determined. Autoradiography, Terminal deoxynucleotidyl transferase dUTP nick end labeling (TUNEL), and cleaved caspase-3 immunostaining were performed on adjacent tumor sections to identify areas of apoptosis.

Results: The *in vitro* cell assays showed caspase-3-dependent uptake of [^{18}F]-CP18 in tumor cells when treated with an apoptosis inducer. The *in vivo* microPET imaging signal of [^{18}F]-CP18 in xenograft tumors correlated with the *ex vivo* caspase-3/7 activities in these tumors. Furthermore, tumor autoradiographies of [^{18}F]-CP18 in tumor sections matched adjacent sections stained by TUNEL and caspase-3 immunohistochemistry (IHC).

Conclusions: [^{18}F]-CP18 demonstrated high affinity and selectivity for activated caspase-3 both *in vitro* and *in vivo*, and the results support [^{18}F]-CP18 as a promising new PET imaging agent for apoptosis.

Key words: [^{18}F]-CP18, Caspase-3, PET imaging, Apoptosis, Caspase imaging

Introduction

The discovery of apoptosis and the concept of programmed cell death is one of the most important advances in biologic research of recent years. Apoptosis generally increases in growing tumors, but can greatly vary among different types of tumors [1–3] or within different grades or stages of the same type of tumor. For example, high-grade lymphomas display a significant higher level of apoptosis than do low-grade lymphomas [2]. The extent of

apoptosis increases with the neoplastic potential of the breast lesion [4]. For patients with head and neck cancer and advanced stage breast cancer, higher levels of activated caspase-3 in tumor tissues correlate with an increased rate of recurrence and death [5]. Radiotherapy and chemotherapy generally kill tumor cells by inducing apoptosis [6]. Therefore, apoptosis can be very useful in diagnosis and treatment monitoring of cancer.

The caspase family plays an essential role in apoptosis by initiating, regulating, and executing downstream proteolytic events that occur during apoptosis [7]. Caspase-3 is one of the key executor cysteine-aspartic acid proteases, which is activated both by the intrinsic and extrinsic apoptosis pathways. Since it is closely linked to apoptosis, the detection of activated

caspase-3, using a substrate approach, can provide valuable *in vivo* information of apoptotic cell death in tissues, even before morphological changes occur. Although radio and chemotherapy trigger different signaling pathways, they converge at the same caspase-dependent execution phase requiring the activation of caspase-3 [8]. In summary, considering the universal role of caspases in apoptosis and especially that of caspase-3 in the final common pathway of programmed cell death, caspase-3 is an attractive target as a diagnostic marker.

Positron emission tomography (PET) is used for staging of cancers, selecting appropriate treatment as well as monitoring treatment, particularly in conjunction with the clinical development of new cancer drugs [9]. Given the importance of being able to image apoptosis, several potential imaging probes have been developed, including annexin-V [10], synaptotagmin I [11], caspase-3 inhibitors based on isatins [12], hydrophobic cations such as ¹⁸F-fluorobenzyl triphenylphosphonium cation (¹⁸F-FBnTP) [13], and ApoSense compounds [14], which all target different processes in the apoptotic cascade [15]. However, no apoptosis PET imaging agent has been approved for clinical use yet.

CP18 is designed as a substrate-based caspase-3 imaging agent. Accordingly, a tetrapeptidic caspase substrate sequence “D-E-V-D” (Asp-Glu-Val-Asp, cf. Figure 1) is the key recognition element. A polyethylene glycol and galactose moiety are attached to facilitate transport across cell membranes and maintain optimal pharmacokinetic properties. Mechanistically, this peptide substrate analog is designed to be able to cross intact plasma membranes. Once inside a cell, the substrate is cleaved in the presence of activated caspase-3, resulting in the accumulation of a more polar DEVD [¹⁸F]-radiolabeled metabolite in the cytoplasm of apoptotic cells or bodies. We have labeled [¹⁸F]-CP18 using a “click radiochemistry” approach [16–18] and demonstrated its preferred specificity for caspase-3. We also describe here the synthesis and radiolabeling of [¹⁸F]-CP18, and its biodistribution and metabolism in mice.

Materials and Methods

Animals and Reagents

Athymic Nude-Foxn1nu mice were purchased from Harlan Laboratories (Indianapolis, IN, USA). Rabbit anti-human cleaved caspase-3 polyclonal antibody was purchased from T Signaling (Danvers, MA, USA). All cell lines were purchased from American Type Culture Collection (ATCC, Manassas, VA, USA). The proteases were purchased from R&D system (Minneapolis, MN, USA) or Clontech (Mountain View, CA, USA). TUNEL kit was bought from Roche Diagnostics (Indianapolis, IN, USA). Alexa 488-conjugated goat anti-rabbit IgG was obtained from Invitrogen (Carlsbad, CA, USA). Human caspase-3 was purchased from EMS Millipore (Billerica, MA, USA). Caspase-3/7 substrate Ac-DEVD-AFC was obtained from AnaSpec (Fremont, CA, USA). All other chemicals and reagents were purchased from Sigma (St. Louis, MO, USA) or Thermo Scientific (Rockford, IL, USA) unless otherwise stated.

Cleavage of CP18 by Caspase-3 Enzyme

To test the ability of activated caspase-3 to cleave the tracer, CP18 (2 nmol) and activated caspase-3 (0.25 U) enzyme were mixed in enzyme assay buffer (150 mM NaCl, 50 mM HEPES, 5 mM EDTA, 1 mM DTT, 10 % glycerol, pH 7.0, and 200 μl) and incubated at 37 °C. At 30, 60, 90, and 120 min, a 20-μl sample was removed, and the accumulation of the cleaved product (DEVD) and the reduction of parental CP18 were analyzed by liquid chromatography/mass spectrometry (LC/MS). The cleavage of CP18 was plotted as the percentage of cleaved substrate versus total substrate over time. The experiment was repeated three times. The average cleavage rate was calculated and expressed as nanomole of cleaved CP18 per hour per unit of caspase-3 enzyme.

Selectivity of CP18 Against a Protease Panel

A panel of 21 proteases comprised of human caspase-1, caspase-3, cathepsin A, cathepsin B, cathepsin C, cathepsin L, dipeptidyl peptidase IV, endothelin converting enzyme-1, granzyme B, kallikrein, matrix metalloproteinase-1 (MMP-1), MMP-9, neurolysin, plasma plasmin, presequence protease, protein C, tumor necrosis factor- α -converting enzyme, thrombin, trypsin, plasma coagulation factor Xa, and plasma coagulation factor XIa was investigated in a digestion assay using LC/MS analysis. CP18 (25 μM) was digested with enzyme (0.1 μg) or without enzyme (control sample) in a total volume of 100 μl for 2 h. The digestion was stopped by deproteination using a chloroform/methanol (1:1) extraction followed by centrifugation at 4 °C for 15 min in a microcentrifuge. The supernatant was then analyzed by LC/MS for the presence of the parental form of CP18 and any cleavage product. The results are expressed as percentage of remaining CP18 after enzymatic digestion versus the total amount of CP18 in the control (without protease).

[¹⁸F]-labeling of CP18

[¹⁸F]-labeling was performed on an automated synthesis module with minor hardware modifications in order to accommodate the volatility of [¹⁸F]fluoropentene, including equipping all vents with a charcoal trap. Cyclotron-produced aqueous [¹⁸F]fluoride ion (1.0 to 2.0 Ci) was passed through an anion exchange resin cartridge (Waters QMA®) to retain the [¹⁸F]fluoride and sequester the [O-18]H₂O for recycling. The [¹⁸F]fluoride was eluted from the cartridge into the primary reaction vessel using a solution of aqueous potassium carbonate (3 mg dissolved in water (0.4 ml)). A solution of Kryptofix® 222 (20 mg) dissolved in acetonitrile (1 ml) was added to the aqueous [¹⁸F]fluoride in the primary reaction vessel. The aqueous [¹⁸F]-fluoride mixture was dried by heating the solution between 68 and 95 °C under a simultaneous reduction of pressure (250 mbar) under a stream of argon. After the mixture was dried, a solution of the tosylate precursor pent-4-yn-1-yl 4-methylbenzenesulfonate (20 mg, 84 μmol), dissolved in tetrahydrofuran (THF) (0.5 ml), was added to the reaction vessel containing the anhydrous [¹⁸F]fluoride. The vessel was heated at 110 ± 5 °C for 3 min. The resultant [¹⁸F]fluoropentene was then distilled from the reaction vessel and bubbled into a secondary reaction container. This container contained a premixed solution of the CP18 azide precursor 18S,21S,24S,27S,30S)-30-((2S,3R,4R,5R,6S)-6-((2-azidoacetamido)methyl)-3,4,5-trihydroxytetrahydro-2H-pyran-2-carboxamido)-27-(2-

carboxyethyl)-21-(carboxymethyl)-24-isopropyl-18-methyl-17, 20,23,26,29-penta-oxo-4,7,10,13-tetra-oxa-16,19,22,25,28-pentaazadotriacontane-1,32-dioic acid) (4 mg, 3.75 μmol) dissolved in CuSO₄ (0.1 M, 300 μl), TBTA (15 mg, 28.2 μmol), sodium ascorbate (40 mg, 201 μmol), DMF (0.1 ml), and MeOH (0.1 ml). The reaction was stirred at room temperature for 30 min. The crude reaction mixture was then diluted with water (4.5 ml) and transferred to an HPLC load loop (5 ml) followed by purification via chromatographic separation. Using a semi-preparative HPLC column (Phenomenex Gemini, C18, 5 μm, 10 × 250 mm) at a flow rate of 5 ml/min, a linear step gradient was employed using the following solvents: 5 % MeCN:95 % aqueous TFA (0.05 %) for 5 min, 10 % MeCN:90 % aqueous TFA (0.05 %) for 5 min, 15 % MeCN:85 % aqueous TFA (0.05 %) for 5 min, 20 % MeCN:80 % aqueous TFA (0.05 %) for 5 min, and 25 % MeCN:75 % aqueous TFA (0.05 %). The product eluted between 28 and 35 min from the time of injection. The purified [¹⁸F]-CP18 fraction collected from the HPLC column was then diluted with water (30 ± 10 ml) and captured onto a C18 SepPak cartridge. The C18 SepPak cartridge was then washed with water (10 ml), followed by an elution with ethanol (0.5–1.0 ml) to release the [¹⁸F]-CP18 from the C18 cartridge. The sample was then diluted with sterile water to afford a final formulation of [¹⁸F]-CP18 in a maximum of 10 % ethanol/90 % water (v/v). The labeling was typically accomplished within 90 min from the end of bombardment in an average radiochemical yield of 40 % (decay corrected). The average specific activity was 1.75 × 10⁵ MBq/μmol.

Cell Uptake of [¹⁸F]-CP18

Apoptosis was induced in cultured U-87MG cells (from human glioblastoma) by exposing the cells to the anti-cancer drug 5-FU (10 μM) for two days in six-well plates. Another group of U87 MG cells was left untreated and served as a control group (*n*=3). Both the induced and control groups of cells were then incubated with [¹⁸F]-CP18 (10 μCi/well) at 37 °C for 2 h. The cells were harvested by spinning them down at 2,000 rpm in a microcentrifuge for 1 min after washing twice with PBS. The cell pellet was counted using a γ-counter (1470 Wizard Gamma Counter, Perkin Elmer, Boston, MA, USA). The cells were then lysed with lysis buffer (0.2 % SDS in 1 × PBS, 100 μl), and the protein concentration was measured with a Bio-Rad protein assay reagent. After normalization by protein concentration, the cell uptake of [¹⁸F]-CP18 was expressed as a fold increase between the 5-FU-induced group versus the control group (defined as 1). In parallel to the above experiments, another set of cultured cells was treated identically and analyzed for caspase-3/7 activity measurements (see below).

[¹⁸F]-CP18 Autoradiography

All animal work was performed in accordance to Siemens MIBR Institutional Animal Care & Use Committee (IACUC) approved procedures. Tumor-bearing mice were established by subcutaneous injection of tumor cells (3–5 million cells) into the shoulder of 4- to 8-week-old male athymic Nude-Foxn1nu mice. Tumor-bearing nude mice were administered with [¹⁸F]-CP18 (250 μCi per mouse in a maximum volume of 200 μl of 10 % aqueous ethanol via the tail vein). Mice were sacrificed after 1 h of tracer uptake, and the tumor tissue was collected, embedded, and frozen in optimal cutting temperature. The frozen tumor samples were then immediately cut into 10-μm sections on a cryotome (Leica Microsystems, Bannockburn, IL, USA).

Autoradiographic images were obtained by placing the tissue sections on an imaging plate (FujiFilm, Tokyo, Japan) and exposed overnight at –80 °C. The imaging plate was then read on an FLA-7000 scanner (FujiFilm, Tokyo, Japan). Adjacent sections were used for caspase-3 IHC and TUNEL double staining (see below).

TUNEL and IHC Staining of Tumor Sections

Frozen tumor sections were air dried for 15 min and then fixed in a 1:1 mixture of acetone–methanol for 10 min at room temperature. Next, the slides were quenched with 3 % hydrogen peroxide/0.3 % goat serum in 1 × PBS for 30 min. After blocking with 5 % goat serum for 60 min at room temperature, the sections were treated with rabbit anti-human cleaved caspase-3 polyclonal antibodies (1:200 diluted) and incubated overnight at 4 °C. The sections were visualized using an Alexa 488-conjugated goat anti-rabbit IgG antibody for 60 min at room temperature. Apoptotic regions were detected on the same sections using a commercial TUNEL kit with a TMR red-tagged dUTP. Sections were then imaged for fluorescence and counterstained with hematoxylin, dehydrated, and mounted using Permount (Fisher Scientific, Fair Lawn, NJ, USA). Merged images of whole tumors were taken using an Axio Imager 2 microscope (Carl Zeiss Inc., Jena, Germany). Microscope settings were held constant throughout the sampling.

Image Analysis

Images of whole tumor sections were first overlaid using Adobe Photoshop to ensure accurate positioning of the same region of interests in all images (i.e., autoradiography, TUNEL, cleaved caspase-3 staining, and hematoxylin staining) from adjacent sections. Each image was divided into a 99-field grid pattern. Thirty-three fields were randomly chosen for side-by-side analysis using Image J software (National Institute of Health, USA). For the autoradiography and TUNEL images, signal intensities (mgv) were measured from regions of interest (ROIs) and normalized to the background signal. For the determination of the percentage of apoptotic cells from the cleaved caspase-3 staining, the positive stained cells and hematoxylin stained cells were counted. The percentage of apoptotic cells was then calculated based on the number of positively stained caspase-3 cells over the number of hematoxylin stained cells within the same ROIs. Corresponding ROIs were drawn in both the cleaved caspase-3/TUNEL staining results and the autoradiography results for each data point for a correlation analysis. Similar analyses of images were also performed on other three U-87 MG tumors.

In vivo PET Imaging

A number of different xenograft tumor types, including A-498 (kidney carcinoma, *n*=6), A-427 (human lung carcinoma, *n*=5), LNCaP (human prostate carcinoma, *n*=4), and PC-3 (human adenocarcinoma, *n*=3), were used for comparison of PET imaging and pathology correlations. All tumors varied in their speed of growth, degree of apoptosis, and caspase-3 activity levels. The skeletal muscle served as the background tissue for normalization in the imaging experiments. For the PET scan, mice were anesthetized with 3 % isoflurane/97 % oxygen and injected with [¹⁸F]-CP18 (250 μCi per mouse in a maximum volume of 200 μl of 10 % aqueous ethanol) via bolus intravenous tail vein injection.

One hour following the administration of the tracer, animals were scanned for 30 min to generate a static PET image (INVEON multimodality microPET scanner, Siemens, Germany). ROIs were visually drawn on the resulting PET images, and the corresponding activity values were reported using ASI Pro microPET analysis software. Tumor uptake was normalized to a similar volume of skeletal muscle and expressed as a tumor/muscle (T/M) ratio. Following the acquisition of the PET image, mice were sacrificed, and tumor plus muscle tissues were collected for analysis of caspase-3/7 activities or tumor autoradiographies.

Caspase-3/7 Activity Assay

The enzymatic activity of caspase-3/7 in cell lysates or tissue homogenates was determined by measuring the kinetic accumulation of the cleaved fluorogenic product AFC. The caspase-3/7 substrate Ac-DEVD-AFC (2 μM), DTT (1 μM), and tumor or cell lysates were mixed in enzyme assay buffer (200 μl), and the AFC release was immediately observed in a SpectraMax M2 spectrofluorometer

(Molecular Devices, Sunnyvale, CA, USA) at Ex = 400/Em = 505 nm at 37 °C. Caspase-3/7 activity was normalized by protein concentration of the cell lysates or tissue homogenates. For cell lysates, caspase-3/7 activity was expressed as a fold increase in the 5-FU-induced group versus the control group (defined as 1), while in tumor homogenates, the results were calculated as T/M ratios to match the [¹⁸F]-CP18 PET uptake results which were also expressed as tumor-to-muscle ratios.

Biodistribution of [¹⁸F]-CP18 in Mice

Twelve male Foxn1nu/nu+ wild-type mice were anesthetized with 3 % isoflurane/97 % oxygen and administered with [¹⁸F]-CP18 (200 μCi per mouse in 10 % aqueous ethanol) via bolus intravenous tail vein injection. Three animals were used per time point. At 30, 60, 90, and 120 min post-injection, whole blood was withdrawn via cardiac puncture, and urine samples were collected via cystocentesis. The animals were then sacrificed. Liver, heart, kidneys, skeletal muscle (right quadriceps), and brain were

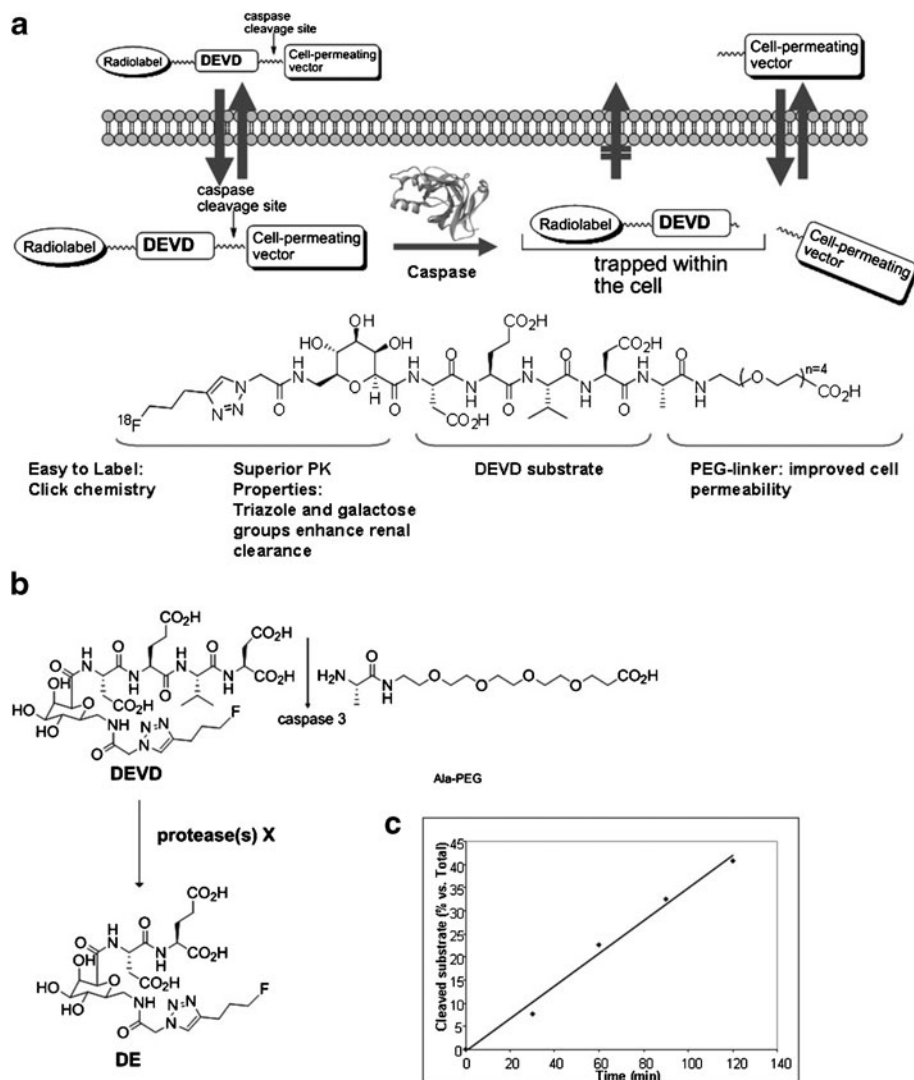


Fig. 1. Caspase-3 substrate-based PET tracer design and cleavage of CP18 by caspase-3. **a** Design of DEVD-based CP18 compound. **b** Cleavage of CP18 by caspase-3 into DEVD and an Ala-PEG linker fragment. DEVD is further cleaved by proteases into DE. **c** Representative kinetic cleavage of CP18 by caspase-3.

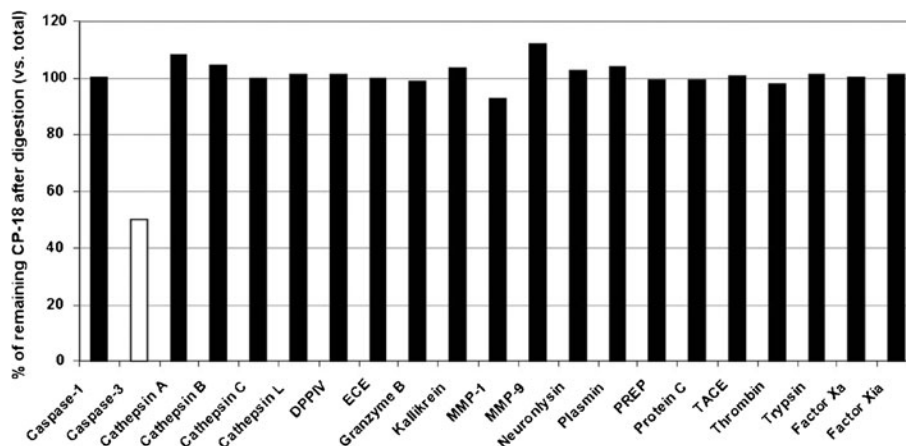


Fig. 2. Enzymatic digestions of CP18 with twenty-one proteases. The results are shown as a percentage of remaining CP18 versus total after 2 h of digestion by different proteases. Only caspase-3 can cleave CP18 (white bar).

harvested and weighed. Each tissue sample was counted on a gamma counter along with an aliquot of the injected dose sample (2 μl). Each data point was converted into the percentage of injected dose per gram of tissue (%ID/g).

Tumor Metabolism of [^{18}F]-CP18 in Mice

U-87 MG tumor-bearing mice were administered with [^{18}F]-CP18 (250 μCi per mouse in a maximum volume of 200 μl of 10 % aqueous ethanol) through the tail vein. Mice were sacrificed 1 h after tracer injection. Plasma and tumor lysates were prepared as described above and processed by adding 8 % acetic acid in acetonitrile (25 μl) to the lysate or plasma samples (100 μl), vortexed at high speed for 1 min, cooled on dry ice for 3 min, thawed, and centrifuged at 13,000 rpm for 7 min. The supernatants were analyzed by HPLC using a radiometric detector (Raytest GmbH, Agilent, Santa Clara, CA, USA).

Statistical Analysis

Data are presented as mean \pm SD unless otherwise stated. Statistical evaluations were performed by analysis of variance. A difference test was done to establish differences between group means. Statistical significance was defined as $P < 0.05$.

Results

Cleavage of [^{18}F]-CP18 by Caspase-3

The structure of [^{18}F]-CP18 is shown in Fig. 1a (MW = 1,152 g/mol). [^{18}F]-CP18 is recognized as a substrate by caspase-3 and cleaved to yield both the [^{18}F]-labeled DEVD fragment and the Ala-PEG linker fragment (Fig. 1b). Our experiments with recombinant caspase-3 showed an expected increase in the DEVD fragment and decrease of parental [^{18}F]-CP18 over time.

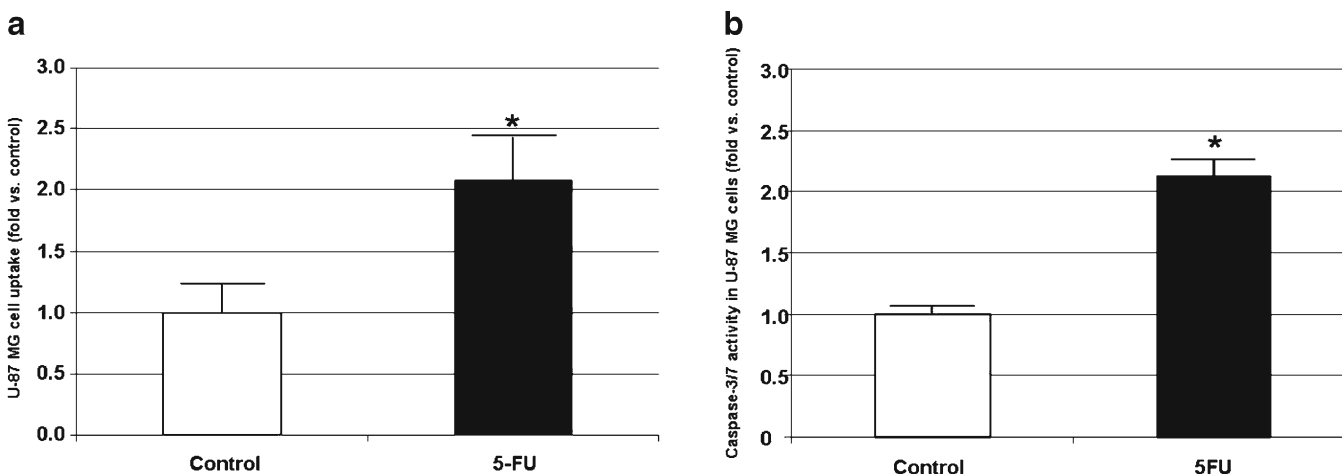


Fig. 3. [^{18}F]-CP18 uptake and caspase-3/7 activity assay in U-87 MG cells. a [^{18}F]-CP18 cell uptake: the uptake in the control group is defined as 1, and after induction with 5-FU, the cell uptake of [^{18}F]-CP18 is about twofold increased. b In parallel, the caspase-3/7 activity was measured. The result is also expressed as the ratio of caspase-3/7 activity post-5-FU treatment over control. $P < 0.05$ ($n=3$).

The cleavage rate of [¹⁸F]-CP18 by recombinant caspase-3 is 1.8 ± 0.3 nmol/h/U ($n=3$, Fig. 1c).

cathepsin B, neurolysin, and granzyme B are known to recognize substrates containing a DEVD sequence, they did not appear to cleave [¹⁸F]-CP18 under these conditions.

Cleavage of [¹⁸F]-CP18 by Other Proteases

The proteolytic stability [¹⁸F]-CP18 was tested against 21 other enzymes, and the results from these digestion assays are shown in Fig. 2. It is apparent that in this selected set of proteases, only caspase-3 significantly cleaved [¹⁸F]-CP18. Even though

Cell Uptake of [¹⁸F]-CP18

We investigated the uptake of [¹⁸F]-CP18 in cells undergoing anti-cancer drug-induced cell death *in vitro* and found that U87 MG cells showed higher [¹⁸F]-CP18 uptake in

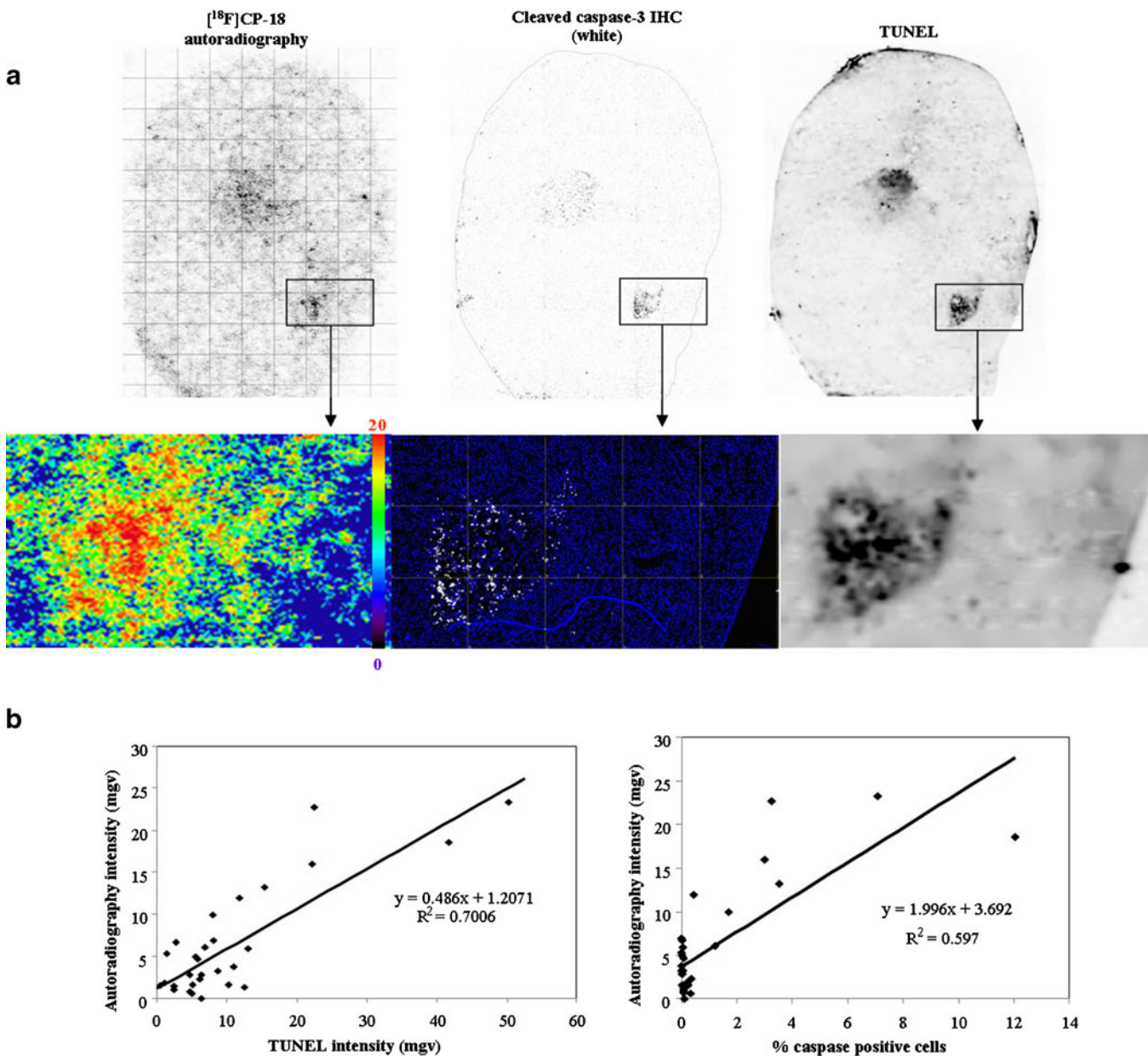


Fig. 4. [¹⁸F]-CP18 autoradiography, cleaved caspase-3 IHC and TUNEL staining images, and the correlations of autoradiography versus IHC and TUNEL staining, respectively. **a** Upper row: representative images of [¹⁸F]-CP18 autoradiography (left), cleaved caspase-3 IHC (middle), and TUNEL (right) staining from adjacent sections of a U-87 MG tumor. Lower row: high magnification from the framed areas. [¹⁸F]-CP18 autoradiography intensity (from 0 to 20) matched positive activated caspase-3 IHC (white; hematoxylin counterstaining was shown as blue) and TUNEL staining. **b** Correlations between autoradiography and TUNEL staining (left) or cleaved caspase-3 IHC (right).

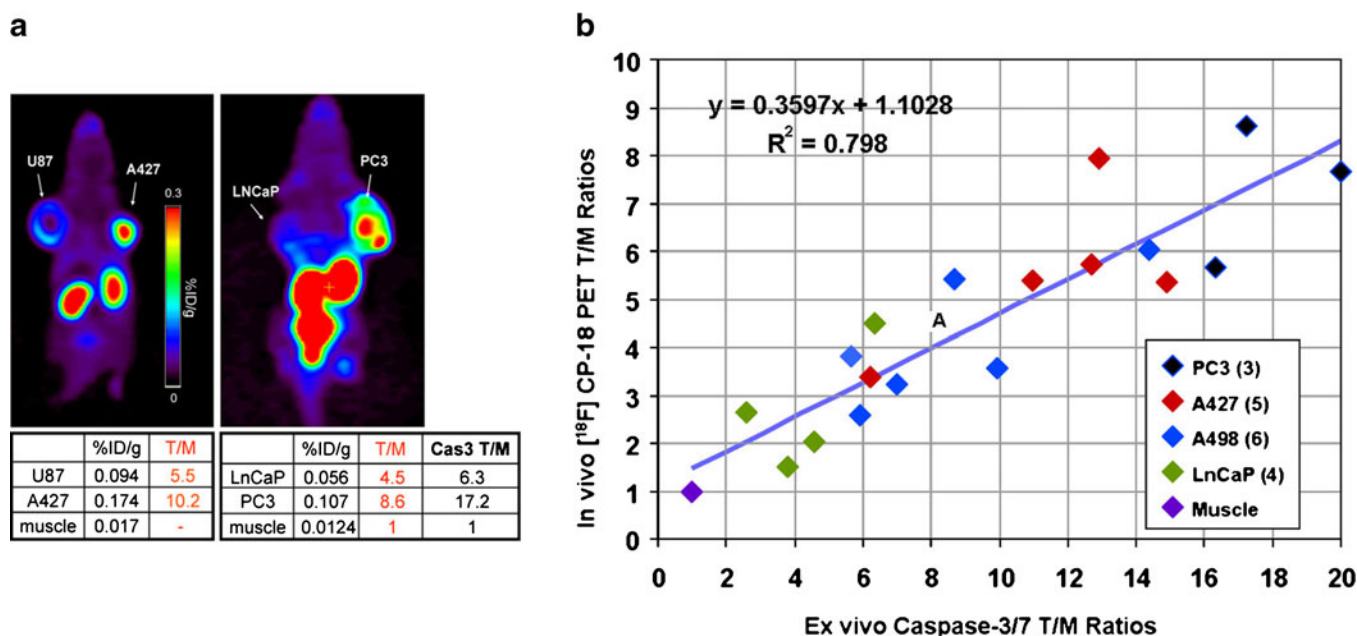


Fig. 5. *In vivo* [¹⁸F]-CP18 PET scans of dual-implant xenograft tumor-bearing mice and caspase-3/7 activity assay in different tumors and muscle. **a** Representative PET images at 60 min post-injection of [¹⁸F]-CP18 (15-min static PET scans). The mouse on the left was carrying U87 (left) and A427 (right) tumors, and the mouse on the right LNCaP (left) and PC3 (right) tumors. **b** A linear correlation of *ex vivo* caspase-3/7 activity T/M ratios and *in vivo* [¹⁸F]-CP18 PET T/M ratios across four different tumor types (A-498 ($n=6$); A-427 ($n=5$); LN CaP ($n=4$); PC-3 ($n=3$)) was observed.

5-FU (a thymidylate synthase inhibitor) treated cells as compared to control cells by up to twofold (Fig. 3a, $n=3$, $P < 0.05$). The relevance of this uptake was confirmed by increased [¹⁸F]-CP18 uptake in 5-FU-treated cells that corresponded to a higher cellular caspase-3/7 activity (Fig. 3b, $n=3$, $P < 0.05$).

Autoradiography, Caspase-3 IHC, and TUNEL Staining

Representative images of U-87 MG tumor sections from [¹⁸F]-CP18 *ex vivo* autoradiographies, caspase-3 IHC, TUNEL, and hematoxylin staining are shown in Fig. 4a. The pattern created by the uptake of [¹⁸F]-CP18 in the tumor generally matched the caspase-3 and TUNEL staining: high intensity areas in the autoradiography section corresponded to more intense TUNEL and caspase-3 staining (Fig. 4a, lower row). A correlation between autoradiographies and TUNEL staining and caspase-3 IHC,

respectively, were calculated and shown in Fig. 4b. Both TUNEL ($R^2 = 0.701$) and activated caspase-3 ($R^2 = 0.597$) stains showed a good correlation with the autoradiography signal from an adjacent tissue section. Similar results were observed in other three U-87 MG tumors. The intensity of [¹⁸F]-CP18 autoradiography on U87 MG tumor correlated well to TUNEL staining ($R^2 = 0.76 \pm 0.06$, $n=4$) and activated caspase-3 IHC ($R^2 = 0.61 \pm 0.15$, $n=4$).

In vivo PET Scans

Figure 5a shows an example of a static PET image of a mouse with dual implanted tumors (U87 tumor on the left and A427 tumor on the right). Even though the uptake values were relatively small (0.1 %ID/g for the U87 tumor; 0.17 %ID/g for A427), the T/M ratios were quite large (U87, 5.5; A427, 10.2) due to the thorough background clearance. In another dual

Table 1. Biodistribution of [¹⁸F]-CP18 in mice

Time (min)	Plasma	Heart	Brain	Liver	Kidneys	Urine	Muscle
30	0.84 ± 0.13	0.24 ± 0.1	0.03 ± 0.01	0.90 ± 1.13	3.75 ± 1.33	590.5 ± 341.4	0.21 ± 0.07
60	0.35 ± 0.00	0.18 ± 0.01	0.06 ± 0.01	0.27 ± 0.01	7.59 ± 1.16	476.8 ± 30.8	0.19 ± 0.02
90	0.14 ± 0.03	0.26 ± 0.05	0.04 ± 0.00	0.35 ± 0.01	7.91 ± 0.46	296.4 ± 153.7	0.07 ± 0.01
120	0.02 ± 0.00	0.08 ± 0.02	0.03 ± 0.01	0.22 ± 0.01	4.57 ± 0.11	55.91 ± 3.70	0.04 ± 0.01

Note: data are expressed as mean ± SD. The values are expressed as %ID/g. $N=3$ for each time point. [¹⁸F]-CP18 is rapidly cleared from the blood stream, and the major elimination pathway of [¹⁸F]-CP18 is through the kidneys and bladder via urine

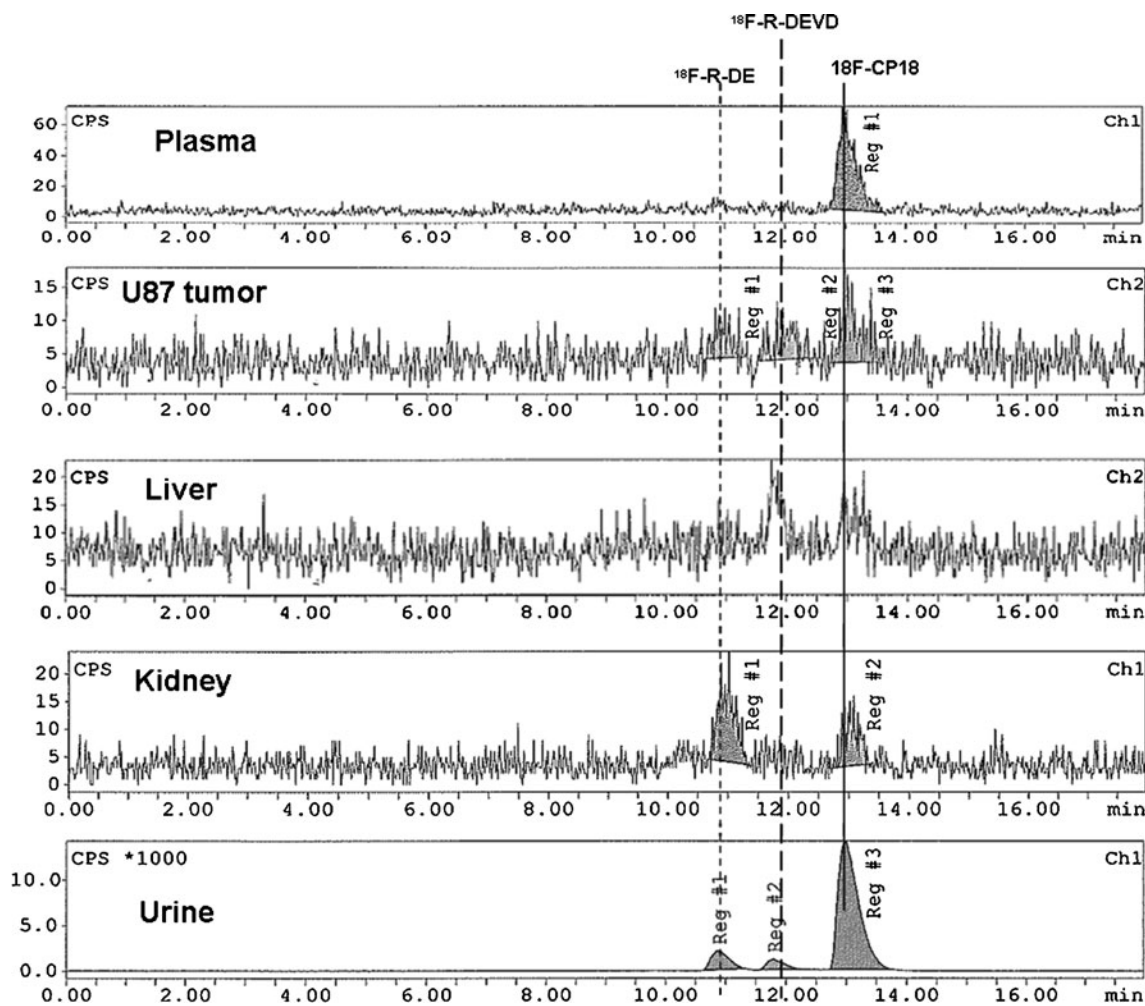


Fig. 6. [¹⁸F]-CP18 tumor metabolism in mice. Representative HPLC analyses of 30-min plasma, tumor, and urine extract samples from mice. The caspase-3-induced hydrolysis product of [¹⁸F]-CP18 is found inside the tumor but not in the plasma.

implant model, the PC3 tumor demonstrated a much higher retention of [¹⁸F]-CP18 (T/M ratio = 8.6; %ID/g = 0.107) and also had elevated caspase-3 activity levels (*ex vivo* caspase-3 activity T/M ratio = 17.2) compared to the LNCaP tumor (T/M ratio = 4.5; %ID/g = 0.056; *ex vivo* caspase-3 activity T/M ratio = 6.3). Results from four different types of tumors (A-498, A-427, LNCaP, and PC-3) and muscle with their corresponding caspase activity levels are shown in Fig. 5b. These tumor types reveal a wide range of different caspase levels, which correlate strongly with the T/M ratios obtained from the PET images. These results clearly demonstrate that [¹⁸F]-CP18 uptake is linked to caspase-3 activity.

Biodistribution and Clearance of [¹⁸F]-CP18 in Wild-Type Mice

[¹⁸F]-CP18 was rapidly cleared from the blood stream in mice, decreasing from 0.84 %ID/g at 30 min to 0.02 %ID/g at 120 min. Elimination via urine was significant, resulting in a

maximum radiotracer concentration of 590 %ID/g at 30 min that decreased to 55 %ID/g at 120 min. The majority of the radiotracer was distributed primarily in the kidneys and to a far lesser extent in the liver. The uptake of radioactivity in the other tissues (brain, heart, and muscle) was less than that observed in the liver (Table 1).

[¹⁸F]-CP18 Metabolism in Tumor and Other Tissues

As shown in Fig. 6, a [¹⁸F]DEVD fragment was formed after caspase cleavage, and further proteolytic digestion resulted in a shorter [¹⁸F]DE cleavage product. At 30 min post-dose, mouse plasma contained mostly unchanged parent (93 %), 7 % of [¹⁸F]DE, and 0.06 % of [¹⁸F]DEVD. In U-87 MG tumors, significant amounts of [¹⁸F]DE (28 %) and [¹⁸F]DEVD (25 %) fragments were formed, while only 47 % of parent [¹⁸F]-CP18 was present. In kidneys, the relative amounts of parent [¹⁸F]-CP18 and [¹⁸F]DE detected in the aqueous fraction of the tissue

were 37 and 63 %, respectively. The aqueous and organic urine fractions contained roughly equal amounts of radioactivity. [¹⁸F]DE, [¹⁸F]DEVD, and parent [¹⁸F]-CP18 were all present in the urine samples with amounts of 11.0 %, 5.4 %ID/g, and 83.6 %, respectively, at the 30-min time points.

Discussion

CP18 contains a caspase-3 substrate sequence, the tetrapeptide “D-E-V-D,” with additional structural elements to support cellular uptake and renal clearance (Fig. 1). To optimize PK properties and clearance of the tracer, several modifications were made and tested, and finally, the hydrophilic 1,2,3-antitriazole and galactose moieties were incorporated for best *in vitro* and *in vivo* results. The addition of the PEG group resulted in increased overall tumor uptake of the tracer ascribable to enhanced cell permeability. Mechanistically, it is desirable for the tracer to be cell permeable, and localization should only occur once the substrate is cleaved, leaving a radiolabeled metabolite trapped intracellularly. A similar approach was reported by Bauer and coworkers [19]. Once [¹⁸F]-CP18 is cleaved by caspase-3, a charged ¹⁸F-labeled DEVD fragment is formed and trapped inside the cytosol. It is therefore possible for the tracer to accumulate in apoptotic cells, resulting in a signal increase relative to non-apoptotic tissues.

As a PET imaging agent of apoptosis, [¹⁸F]-CP18 successfully satisfies several criteria for quantitative imaging of apoptosis. First, CP18 demonstrated a high selectivity and specificity for its target (active caspase-3). *In vitro* studies confirmed that CP18 is cleaved only by caspase-3 and stable in the presence of other proteases, including cathepsin B, neurolysin, and granzyme B, which can cleave substrates containing a DEVD sequence. *In vivo*, the uptake of [¹⁸F]-CP18 in various mouse xenograft tumors correlated with caspase-3 activity. Tumor tissue sections were prepared and further investigated by autoradiography, TUNEL, and caspase-3 IHC. The good overlap between hot autoradiographic areas and caspase-3 IHC as well as TUNEL staining further confirms CP18’s specific enrichment in caspase-3 containing areas. Secondly, this PET imaging agent demonstrates suitable *in vivo* properties: caspase-3 activity in different tumor types results in a favorable signal-to-background ratio in mice xenograft tumors, along with a fast distribution and rapid clearance from non-target tissues. There was a good match of [¹⁸F]-CP18 in different types of tumors with caspase-3 activity in tumor lysates. We attempted to induce apoptosis in mouse xenograft models with various cancer agents, such as 5-FU or doxorubicin. However, we found that the baseline caspase activity in these fast growing xenograft tumor models was very high already and varied greatly from animal to animal even within the same tumor cell line. It was difficult, therefore, to obtain a stable tumor model for chemotherapy-induced apoptosis, and we decided to focus on determining the correlation of caspase-3 activity with tracer uptake, as well as testing [¹⁸F]-CP18 in a dexamethasone thymus apoptosis

model (cf., companion article, which precedes the current one). However, as tumors in cancer patients are quite different from xenograft models, we hope that the correlation of caspase activity and PET signal will be evident in a treatment that induces apoptosis in humans. In addition to treatment monitoring, we propose that [¹⁸F]CP18 may also be useful as a tool for diagnosis of cancers. Thirdly, [¹⁸F]-CP18 showed good plasma biostability with minimal metabolism evident, except in tissues with elevated caspase activity, such as in tumors.

Currently, apoptosis imaging agents can be classified into four categories based on their mechanism of action or biochemical target: plasma membrane phospholipid asymmetry and phosphatidylserine exposure (such as annexin-V, synaptotagmin I) [10, 11], caspase activation (such as caspase-3 inhibitor, isatin-based tracers) [12, 20], collapse of mitochondrial membrane potential (such as FBnTP) [13], and finally others without a known target or mechanism (such as ApoSense compounds) [21]. Two tracers, annexin-V and ML-10, have been investigated clinically [22, 23], and [^{99m}Tc]-annexin-V is one of the earliest probes developed for apoptosis imaging. However, its performance *in vivo* is moderate [24], partially due to non-specific uptake [25, 26] as well as pharmacokinetic problems associated with a relatively large protein (36 Kd) such as slow clearance from the blood. Lack of a correlation between uptake and patient outcome was reported in head and neck cancer patients with chemoradiotherapy treatment [27]. [¹⁸F]ML-10 was the first in class PET imaging agent for drug-induced apoptosis to enter clinical trials. However, the mechanism of apoptotic cell binding is unproven, and at this point, the use of this imaging agent is more empiric than mechanistically based.

There is a need for new mechanism-based PET imaging agents to detect and monitor apoptosis. [¹⁸F]-CP18 is a substrate-based agent designed to image apoptotic cells. It is designed to distribute reversibly into cells but trapped specifically within cells with active caspase-3. The presence of the expected metabolic cleavage products in apoptotic cells and tissues further confirms the mechanism of action. Its uptake correlates with caspase-3 activity and shows a superior imaging profile.

Conclusion

Here, we have shown that the uptake of [¹⁸F]-CP18 in apoptotic cells *in vitro* and *in vivo* is mechanism-based and specific. [¹⁸F]-CP18 is cleaved by active caspase-3, taken up by apoptotic tumor cells and rapidly cleared from non-target tissues. [¹⁸F]-CP18 is currently being developed clinically as a positron emitting radiopharmaceutical for imaging of apoptosis.

Conflict of Interest. The authors declare that they have no conflict of interest.

References

1. Soini Y, Virkajarvi N, Lehto VP, Paakko P (1996) Hepatocellular carcinomas with a high proliferation index and a low degree of apoptosis and necrosis are associated with a shortened survival. *Br J Cancer* 73:1025–30

2. Soini Y, Raunio H, Paakko P (1998) High-grade malignant non-Hodgkin's lymphomas differ from low-grade lymphomas in the extent of apoptosis and their expression of bcl-2, mcl-1, bax and p53. *Tumour Biol* 19:176–85
3. Tormanen U, Eerola AK, Rainio P, Vahakangas K, Soini Y, Sormunen R et al (1995) Enhanced apoptosis predicts shortened survival in non-small cell lung carcinoma. *Cancer Res* 55:5595–602
4. Mustonen M, Raunio H, Paakko P, Soini Y (1997) The extent of apoptosis is inversely associated with bcl-2 expression in premalignant and malignant breast lesions. *Histopathology* 31:347–54
5. Huang Q, Li F, Liu X, Li W, Shi W, Liu FF et al (2012) Caspase 3-mediated stimulation of tumor cell repopulation during cancer radiotherapy. *Nat Med* 17:860–6
6. Hersey P, Zhang XD (2003) Overcoming resistance of cancer cells to apoptosis. *J Cell Physiol* 196:9–18
7. Riedl SJ, Shi Y (2004) Molecular mechanisms of caspase regulation during apoptosis. *Nat Rev Mol Cell Biol* 5:897–907
8. Taylor RC, Cullen SP, Martin SJ (2008) Apoptosis: controlled demolition at the cellular level. *Nat Rev Mol Cell Biol* 9:231–41
9. Wahl RL, Jacene H, Kasamon Y, Lodge MA (2009) From RECIST to PERCIST: Evolving considerations for PET response criteria in solid tumors. *J Nucl Med* 50(Suppl 1):122S–50S
10. Yagle KJ, Eary JF, Tait JF et al (2005) Evaluation of ¹⁸F-annexin V as a PET imaging agent in an animal model of apoptosis. *J Nucl Med* 46:658–66
11. Zhu X, Li Z, Zhao M (2007) Imaging acute cardiac cell death: temporal and spatial distribution of ^{99m}Tc-labeled C2A in the area at risk after myocardial ischemia and reperfusion. *J Nucl Med* 48:1031–6
12. Chen DL, Zhou D, Chu W et al (2009) Comparison of radiolabeled isatin analogs for imaging apoptosis with positron emission tomography. *Nucl Med Biol* 36:651–8
13. Madar I, Huang Y, Ravert H et al (2009) Detection and quantification of the evolution dynamics of apoptosis using the PET voltage sensor ¹⁸F-fluorobenzyl triphenyl phosphonium. *J Nucl Med* 50:774–80
14. Cohen A, Shirvan A, Levin G et al (2009) From the Gla domain to a novel small-molecule detector of apoptosis. *Cell Res* 19:625–37
15. Reshef A, Shirvan A, Akselrod-Ballin A et al (2010) Small-molecule biomarkers for clinical PET imaging of apoptosis. *J Nucl Med* 51:837–40
16. Kolb HC, Finn MG, Sharpless KB (2001) Click chemistry: diverse chemical function from a few good reactions. *Angew Chem Int Ed Engl* 40:2004–21
17. Tornøe CW, Christensen C, Meldal M (2002) Peptidotriazoles on solid phase: [1,2,3]-triazoles by regioselective copper(I)-catalyzed 1,3-dipolar cycloadditions of terminal alkynes to azides. *J Org Chem* 67:3057–64
18. Rostovtsev VV, Green LG, Fokin VV, Sharpless KB (2002) A stepwise Huisgen cycloaddition process: copper(I)-catalyzed regioselective “ligation” of azides and terminal alkynes. *Angew Chem Int Ed Engl* 14:2596–9
19. Bauer C, Bauder-Wuest U, Mier W et al (2005) ¹³¹I-labeled peptides as caspase substrates for apoptosis imaging. *J Nucl Med* 46:1066–74
20. Nguyen QD, Challapalli A, Smith G et al (2012) Imaging apoptosis with positron emission tomography: ‘bench to bedside’ development of the caspase-3/7 specific radiotracer [¹⁸F]ICMT-11. *Eur J Cancer* 48:432–40
21. Allen AM, Ben-Ami M, Reshef A et al (2012) Assessment of response of brain metastases to radiotherapy by PET imaging of apoptosis with (18)F-ML-10. *Eur J Nucl Med Mol Imaging* 39:1400–8
22. Belhocine T, Steinmetz N, Hustinx R et al (2002) Increased uptake of the apoptosis-imaging agent (99m)Tc recombinant human annexin V in human tumors after one course of chemotherapy as a predictor of tumor response and patient prognosis. *Clin Cancer Res* 8:2766–74
23. Hoglund J, Shirvan A, Antoni G et al (2011) ¹⁸F-ML-10, a PET tracer for apoptosis: first human study. *J Nucl Med* 52:720–5
24. Vermeersch H, Loose D, Lahorte C et al (2004) ^{99m}Tc-HYNIC annexin-V imaging of primary head and neck carcinoma. *Nucl Med Commun* 25:259–63
25. Kemerink GJ, Liu X, Kieffer D et al (2003) Safety, biodistribution, and dosimetry of ^{99m}Tc-HYNIC-annexin V, a novel human recombinant annexin V for human application. *J Nucl Med* 44:947–52
26. Rottey S, Van den Bossche B, Slegers G et al (2009) Influence of chemotherapy on the biodistribution of [^{99m}Tc]hydrazinonicotinamide annexin V in cancer patients. *Q J Nucl Med Mol Imaging* 53:127–32
27. Hoebbers FJ, Kartachova M, de Bois J et al (2008) ^{99m}Tc Hynic-rh-annexin V scintigraphy for *in vivo* imaging of apoptosis in patients with head and neck cancer treated with chemoradiotherapy. *Eur J Nucl Med Mol Imaging* 35:509–18
28. Faust A, Wagner S, Law MP et al (2007) The nonpeptidyl caspase binding radioligand (S)-1-(4-(2-[¹⁸F]fluoroethoxy)-benzyl)-5-[1-(2-methoxymethylpyrrolidinyl)sulfonyl]isatin ([¹⁸F]CbR) as potential positron emission tomography-compatible apoptosis imaging agent. *Q J Nucl Med Mol Imaging* 51:67–73